CHARACTERIZATION OF A DUAL OPTO-MECHANICAL RESONATOR FOR INERTIAL SENSING

A Thesis

by

LEE ANN CAPISTRAN

Submitted to the Graduate and Professional School of
Texas A&M University
in partial fulfillment of the requirements for the degree of

MASTER OF SCIENCE

Chair of Committee,	Felipe Guzman
Committee Members,	Jose Sanjuan Munoz
	Chandler Benjamin
Head of Department,	Ivett Leyva

May 2023

Major Subject: Aerospace Engineering

ABSTRACT

Accelerometers are key sensors in many fields and applications such as precision metrology, gravimetry measurements, gravitational wave observatories, and navigation where position and attitude need to be determined accurately. A combination of at least six accelerometers provides all the necessary information to estimate position and orientation of a rigid body and thus serves as an inertial navigation system for autonomous navigation. Fused-silica based mechanical resonators paired with laser interferometric read-outs enable compact high-precision accelerometers. I will present my work on the development of a wide-band accelerometer based on a double resonator with two test masses of different sizes in a single frame. One of the resonators has a resonance frequency of about 50 Hz, while the other is optimized for lower frequencies and has a nominal frequency of about 10 Hz. The combination of the two resonators allows for excellent long-term precision while maintaining good measurement bandwidth. Using a free-space heterodyne laser interferometer and fiber-based heterodyne interferometer, characterization of the system in air and in vacuum has been conducted. The calculated and expected performance will be presented along with the experimental procedure.

DEDICATION

To my son and younger self.

ACKNOWLEDGMENTS

I would like to thank my committee chair, Dr. Felipe Guzman, for always supporting me, encouraging me and guiding me through the hardest parts of my academic career. My committee members Dr. Jose Sanjuan for having patience while I learned about my research and teaching me the concepts I need, and Dr. Chandler Benjamin for being an excellent professor and encouraging me to continue my education.

I would also like to thank my mother Angie, my grandparents Mario and Maria, my brother Eric, sister in law Casy, and sister Valentina, for their endless emotional support and encouragement through my academic journey and shared excitement about my successes. I want to thank my fiance, Isaac, and son for being my source of happiness when I get home and for their love and motivation. I want to also thank my best friends, Erika and Paulina who even from a distance knew I would succeed, and Brina for making sure I don't go through my semesters alone. I would like to thank my dungeons and dragons group, Lucia, Alex, Julie and Logan for providing moral and emotional support when I needed it most and helping me escape reality from time to time, and my cats Saturn and Jupiter for easing my anxiety with kisses and cuddles.

I would like to thank the friends I have made along the way who I have made many memories with: Xiangyu, Andrea, Yanqi, Alberto, Conrad, Ian, Edo, David, Grigory, Giorgi, Pen, Jackson, Momo and Adam. Lastly, I would like to thank the department faculty and staff for making my time at Texas A&M University an experience I will never forget.

CONTRIBUTORS AND FUNDING SOURCES

Contributors

This work was supported by a thesis committee consisting of Professor Dr. Felipe Guzman and Dr. Jose Sanjuan of the Department of Aerospace Engineering and Dr. Chandler Benjamin of the Department of Mechanical Engineering.

The double resonator presented in this thesis was developed by Dr. Adam Hines. The quasi-monolithic, compact, and fiber-based heterodyne interferometers were developed by Dr. Yanqi Zhang. Characterization of the quasi-monolithic interferometer unit is being carried out by Ian Harley-Trochimczyk and Dr. Xiangyu Guo. Initial alignment of the fiber-based interferometer was carried out in part by Dr. Guillermo Valdes and the integration of the fiber-based interferometer was carried out by the student. Guidance on alignment and data processing has been provided by Dr. Xiangyu Guo, Dr. Adam Hines and Dr. Jose Sanjuan. All other work conducted for the thesis was completed by the student independently.

Funding Sources

Graduate study was supported by an assistant-ship from Dr. Felipe Guzman and funding from the National Science Foundation (NSF) (grant PHY-2045579).

TABLE OF CONTENTS

Page

LIST OF FIGURES

FIGURE Page

1. INTRODUCTION*

[1] Accelerometers are present in a large variety of applications and fields where precise measurements of vibrations and non-inertial accelerations are needed. These include gravimetry and seismometry applications, vibration measurements in ground-based gravitational wave detectors, and inertial navigation, among others. Inertial navigation allows users to identify an objects orientation and position without the need of any external information provided to the system or global navigation satellite systems availability. It is important for the inertial sensors to have low noise floor limits. A noise floor refers to the noise that a system produces itself. Reducing a system's noise floor allows for higher sensitivity to vibrations outside of the system. A system with a low noise floor provides higher accuracy allowing for longer autonomous navigation. Accelerometers are critical parts of inertial navigation units, where the linear acceleration is measured and used to estimate the position of the body. Presented is a dual optomechanical accelerometer that includes two resonators with different resonance frequency. The low-frequency one exhibits a high-sensitivity at the expense of a small bandwidth (around a few Hertz). The second resonator, with a higher resonance frequency, complements the low-frequency one and aids measuring accelerations at short time scales (up to hundreds of milliseconds). Optomechanics, as the name implies, combines mechanical and optical design. Examples of applications of optomechanics includes lenses, cameras, microscopes, and it can used to observe the interaction of light and mechanical motion. Optomechanical systems have the capability of being precise and measuring small displacements. Resonators are devices that oscillate, in our case mechanically, with greater amplitude at certain frequencies, or their resonant frequency. Our optomechanical resonators are fabricated from single fused-silica wafers with a test mass anchored to a frame through leaf-spring flexures. The length of the flexures (among other parameters) define the resonance frequency of the resonator. The motion

[1]*Reprinted with permission from "Wide-band dual optomechanical resonators for inertial navigation" by Lee A. Capistran, Adam Hines, Jonathan Joseph Carter, Xiangyu Guo, Guillermo Valdes, Jose Sanjuan, Felipe Guzman Proceedings Volume 12447, Quantum Sensing, Imaging, and Precision Metrology; 1244718 (2023) SPIE Quantum West, 2023

of the resonators is sensed using laser heterodyne interferometry [2, 3], which can be converted to acceleration by knowing the transfer function of the resonator. Characterizing the optomechanical double resonator will confirm its performance as an inertial sensor. Resonance frequencies and quality factors, Q, have been measured using different optical read-out and different conditions. The resonant frequency, ω_0, of a resonator represents the natural frequency at which the resonator operates at. This also identifies the resonators operational bandwidth. Fast and quick changes in acceleration can be measured by a system with higher ω_0 while slow accelerations can be measured with a lower ω_0, and if put together as one single unit they would help in canceling out common noise in a system.

To outline this paper: Chapter 2 will give information on the approach being used along with background information on the techniques and systems used. The results in the experiment both in air and in vacuum will be presented in Chapter 3. The challenges faced and measured and projected noise floors will also be presented in this chapter. Lastly the 4^{th} chapter will consist of a conclusion.

2. APPROACH

In order to characterize the double resonator, interferometric read out systems were implemented. These optical read out systems allow for high sensitivity, low noise floors, and are unaffected by surrounding magnetic fields. These characteristics make optical read out systems good candidates for situations where precise measurements of acceleration are needed.

2.1 Double Resonator

The double resonator is an optomechanical resonator of two test masses on a frame made of a single piece of fused silica. The choice to use fused silica was made based on fused silica's low loss properties at room temperature and the fact that it is not susceptible to surrounding magnetic fields. Figure 2.1 shows the dual optomechanical resonator. The resonator with *short* flexures (30 mm) is designed to have a resonance frequency around 50 Hz. The other resonator, with flexures about 72 mm in length, has a nominal resonance frequency of 10 Hz. Both test masses weigh 2.2 g. This allows for a compact foot print, high bandwidth. The 10 Hz resonator's longer flexures allow for slower oscillations therefore having a lower resonant frequency. Meanwhile, the shorter flexures resonate at a higher frequency because the oscillations are short and quick. This dual configuration can be advantageous for inertial navigation to increase accuracy at long-time scales while maintaining the ability to measure sudden and fast acceleration signals present in vehicles or any body in general. This also means that both resonators have the potential of measuring the same environmental vibrations that can be subtracted from data post processing. This becomes useful when characterizing the resonator's noise floor. Very different applications, such as seismic environmental monitoring in ground-based gravitational wave detectors, can also benefit from such accelerometers, where vibrations up to 30 Hz degrade the observatory performance [4].

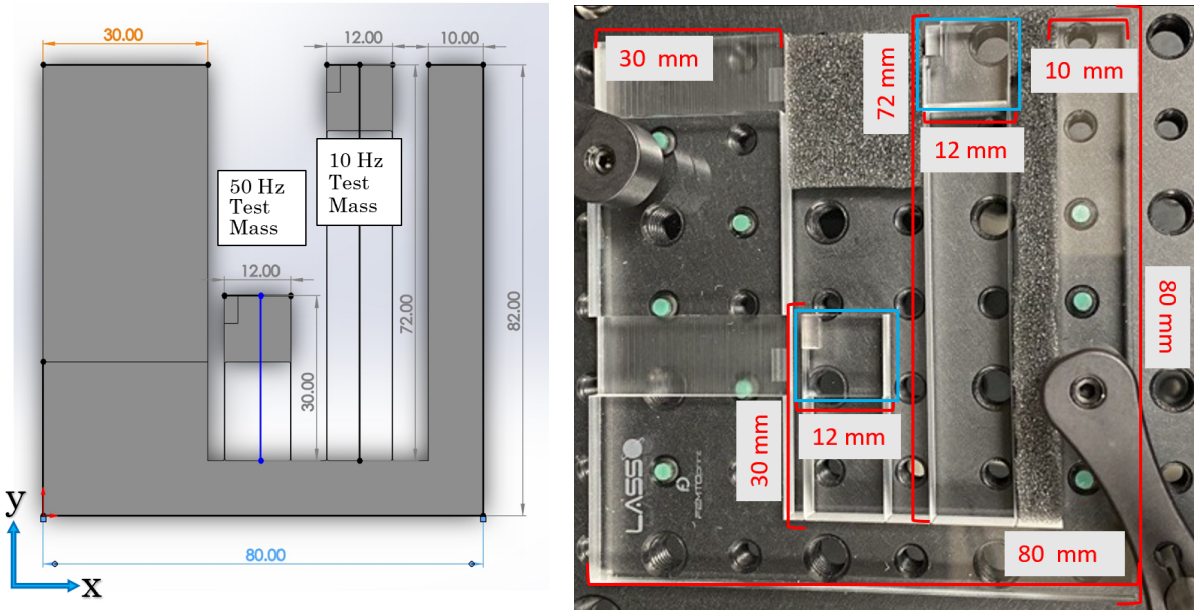

Figure 2.1: This is the 3D model of the double resonator with dimensions. All dimmensions are in mm. The thickness of the resonator is 7 mm. The thickness of the flexures is 100μm. The direction of the motion is in the x-direction.

2.2 Interferometry and Readout

Characterization of the double resonator will give us an understanding of what its capabilities as an inertial sensor are. In order to carry out the characterization, the double resonator was paired with optical readout systems. Interferometric readout systems used with our system include a fiber-based heterodyne interferometer [3], compact heterodyne interferometer [1], and quasi-monolithic interferometer [5]. These interferometers were chosen for their ability to be compact and the levels of sensitivity that can be achieved with them. In order to protect the double resonator, custom-made aluminum housing system was designed and fabricated out of aluminum 6063 T4. This mount houses the optical components required for the compact optical readout systems. Ball-bearing point set screws were chosen to hold the resonator in place inside the mount, while minimizing the contact between the housing and the double resonator. This is to limit parasitic effects that could degrade the mechanical quality factors. For example, if the housing system had a resonant

frequency close to the resonator's, the vibrations of the housing system would couple into our data possibly dominating the data taken by the resonators. Another example is, if the mount had more points of contact, it may contribute to surface losses. However, using multi-physics software, like Solidworks and Comsol, the resonant frequency of the mount was simulated and found to be 2000 Hz, well above the double resonators resonant frequency. This housing system also allows for stability of the resonator to keep it from misalignment during measurements.

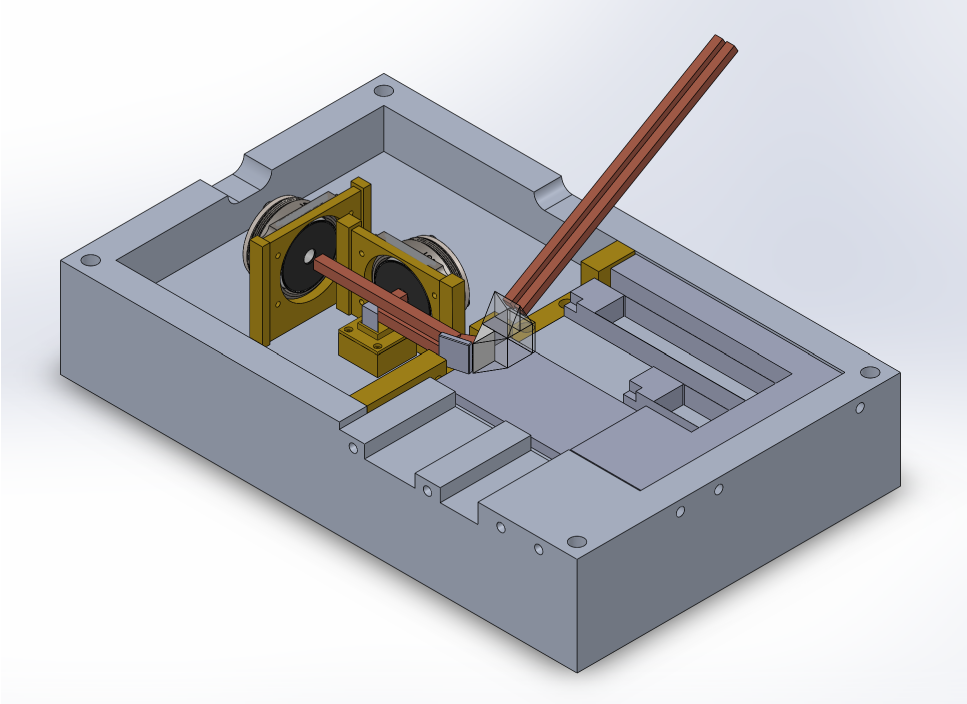

Figure 2.2: CAD file of mount with attachments in place (indicated in gold) and the beam path as well (indicated in red) and fabricated mount without the lid and resonator sitting inside of it. This image is reprinted with permission from "Wide-band dual optomechanical resonators for inertial navigation" by Lee A. Capistran, Adam Hines, Jonathan Joseph Carter, Xiangyu Guo, Guillermo Valdes, Jose Sanjuan, Felipe Guzman Proceedings Volume 12447, Quantum Sensing, Imaging, and Precision Metrology; 1244718 (2023) SPIE Quantum West, 2023

Measurements of acceleration in air were done using a fiber based heterodyne interferometer integrated with the 10 Hz test mass and a compact heterodyne interferometer with common-mode differential optical paths for the 50 Hz test mass. The compact heterodyne interferometer works

by splitting two frequency-shifted beams into two heterodyne interferometers, allowing for spatial separation of the beams. The two paths of the compact heterodyne interferometer are the so called measurement and reference paths. The latter is used to subtract the common environmental noise picked up from the fibers or other common paths. One tracks the test mass motion by reflecting a beam off a mirror on the test mass. The other interferometer reflects a beam off a stationary reference mirror to make a second simultaneous measurement of noise in the optical readout. A differential phase measurement of the two interferometers rejects any common-mode noise to improve the displacement sensitivity. In this set-up, a 633 nm Helium Neon laser source was integrated with the compact heterodyne interferometer [3] and the 50 Hz resonator. Two acousto-optic modulators (AOMs) modulated the source at 80 MHz and 85 MHz, respectively, to generate a heterodyne signal at 5 MHz. Past the AOMs, the two beams have a vertical separation of 15 mm. The design for the interferometer unit, along with its integration with the double resonator, and the beam path followed within, is shown in Fig. 2.3 (top). The optical path inside the interferometer is as follows:

- First the 2 initial beams with frequencies 80 and 80 MHz, respectively, pass through the initial beam splitter (BS1). This beam splitter is turned 45°about the Y axis. The 2 initial beams are split into 4 beams. The four beams are linearly polarized such that they are transmitted through PBS
- Exiting BS1 the 4 beams enter the polarizing beam splitter (PBS)
- Past the PBS all 4 beams pass through a quarter wave plate (QWP)
- Past the QWP the bottom beams are reflected back from a fixed mirror. One of the top beams are reflected from a reference mirror and the other is reflected from the measurement mirror which in this case is a mirror mounted to the arm of the resonator.
- Once reflected back the 4 beams are reflected from the polarizing beam splitter and pass through the second beam splitter (BS2). BS2 has been rotated about the X axis by 90°and about the Z axis by 45°

Details can be found in Ref. [1].

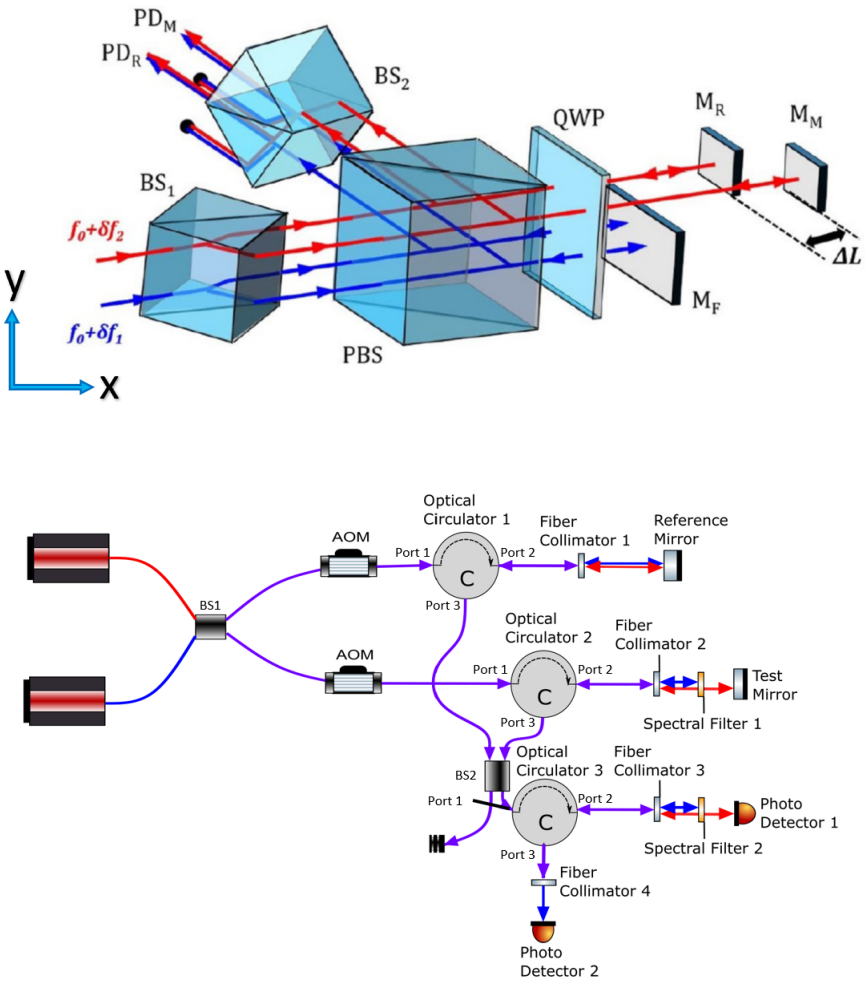

Figure 2.3: Top: Beam path within the compact interferometer unit [1]. Bottom: A simplified schematic of the fiber interferometer. Red and blue representing two different wavelengths (1064 nm and 1055 nm) and purple representing the beams traveling through the same optical fiber. This image is reprinted with permission from "Wide-band dual optomechanical resonators for inertial navigation" by Lee A. Capistran, Adam Hines, Jonathan Joseph Carter, Xiangyu Guo, Guillermo Valdes, Jose Sanjuan, Felipe Guzman Proceedings Volume 12447, Quantum Sensing, Imaging, and Precision Metrology; 1244718 (2023) SPIE Quantum West, 2023

For the 10 Hz resonator, a fiber based heterodyne interferometer [3] was used. This interfer-

ometer uses two wavelengths (1064 nm and 1055 nm) from two different sources. Similar to the compact heterodyne interferometer, one arm of the fiber-based interferometer measures the displacement of the resonator arm, while the other is used to monitor common-mode noise of the fiber system. The two initial beams are driven at 99 MHz and 100 MHz using two AOMs. The optical path followed within the fiber-based heterodyne interferometer is as follows:

- Two beams of different wavelengths are provided by different sources where they are passed through a fiber beam splitter (BS1) first.
- Each ouput arm of the beam splitter are passed through two AOM's to created a heterodyne signal of 1 MHz.
- One AOM out put will be passed through Port 1 of the first optical circulator (OC1).
- Port 2 of OC1 will exit the fiber into free space where both wave lengths will be reflected from a reference mirror entering back through Port 2 of OC1.
- Once both wavelengths enter through Port 2 of OC1 they will pass through Port 3 of OC1 into a second fiber beam splitter (BS2). One output arm of BS2 is discarded while the other enters through the third circulator of the system (OC3).
- Past the second AOM the beam will be imputed to the second circulator of the system (OC2). The two wavelengths will exit into free space via port 2 of OC2. Spectral filter 1 (SF1) is a filter that allows one wavelength (1064 nm) to pass through while reflecting the other wavelength (1055 nm) without passing it through the filter. One wavelength will be reflected off SF1 reentering Port 2 of OC2 while the second wavelength will pass through SF1 and be reflected off the mirror that is mounted to the test mass also re-entering OC2 through Port 2.
- Once both wavelengths enter through Port 2 of OC2 they will pass through Port 3 of OC2 into BS2 where it joins the light from OC1's Port 3 output in entering OC3.
- Port 2 of OC3 will be outputted through free space. One wavelength (1064 nm) will pass through the second spectral filter of the system (SF2) and enter the first photo detector (PD1)

where interference will take place between two beams of the same wavelength but frequency shifted by 99 and 10 MHz. PD1 measures the difference in phase between the reference mirror and the test mirror making it the measurement arm.

- The second wavelength (1055 nm) will reflect off SF2 and reenter OC3 via Port 2 where it will then exit through Port 3 into the second photo detector (PD2) measuring the interference in the same way as the one detected in PD1. PD2 measures the difference in phase between the reference mirror and the fixed mirror making it the reference arm.

Details about this design can be found in Ref. [3], and a simplified diagram is shown in Fig. 2.3 (bottom).

Measurements of acceleration in vacuum call for a more compact system. In order to achieve a compact system, mounting attachments for collimators and a 90°prism were implemented in the design and mounted on the aluminium housing (see Fig. 2.4).

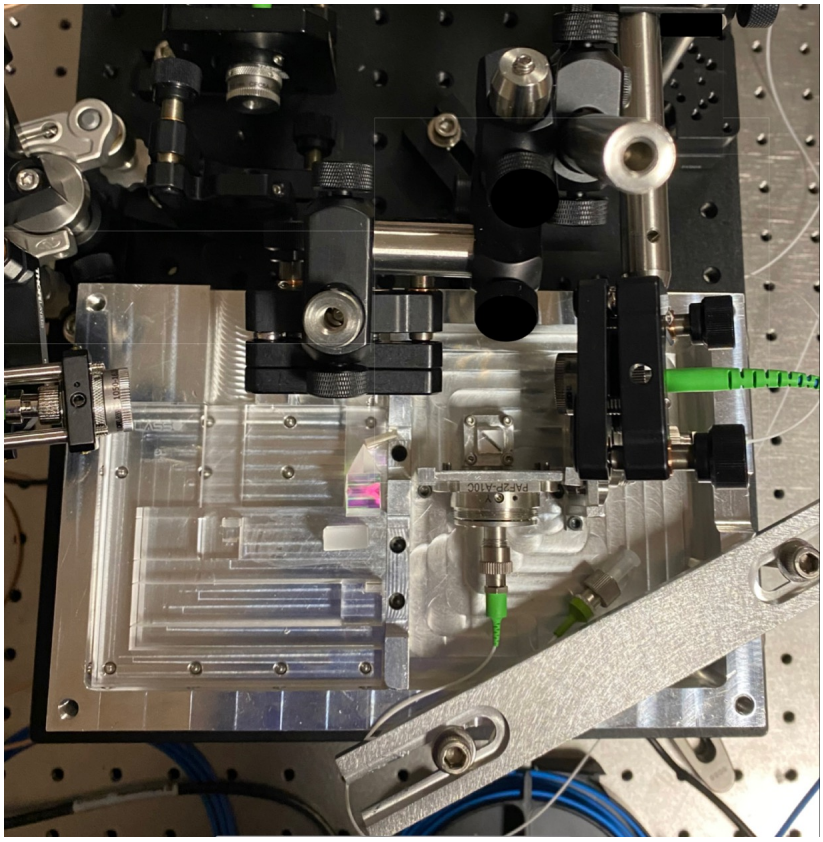

Figure 2.4: All attachments are assembled in the places they should be and both resonators have their respective interferometer integrated. This image is reprinted with permission from "Wide-band dual optomechanical resonators for inertial navigation" by Lee A. Capistran, Adam Hines, Jonathan Joseph Carter, Xiangyu Guo, Guillermo Valdes, Jose Sanjuan, Felipe Guzman Proceedings Volume 12447, Quantum Sensing, Imaging, and Precision Metrology; 1244718 (2023) SPIE Quantum West, 2023

A quasi-monolithic interferometer [2, 5] was mounted on the double resonator itself as shown in Fig. 2.6. This unit is a custom made compact heterodyne interferometer, which has a much smaller footprint than the one used for initial testing in air. The optical path taken by the beams is as follows and can be seen in 2.5:

- The two beams enter through the first equilateral triangular prism (ETP) with a vertical separation of 2.5 mm through the part of the ETP that is coated an anti-reflectivity coating.
- Inside this ETP the beams get split into 4 beams, are reflected by the parts of the ETP coated

with high-reflectivity coating and they will travel through the polarizing beam splitter

- once passing the polarizing beam splitter the top beams get reflected off the reference mirror attached to the quasi-monolithic interferometer.
- Both bottom beams exit the unit through an attached quarter wave plate 1 mm thick. Then one is reflected back into the system by a fixed mirror and the other is reflected back into the system by the measurement mirror on the the test mass.
- Once the beams reenter the PBS where they are directed to the second ETP that rests on top of the system. Both the reflection from the measurement and fixed mirror are combined with one arm of the reference mirror each.
- This is where the lights are detected

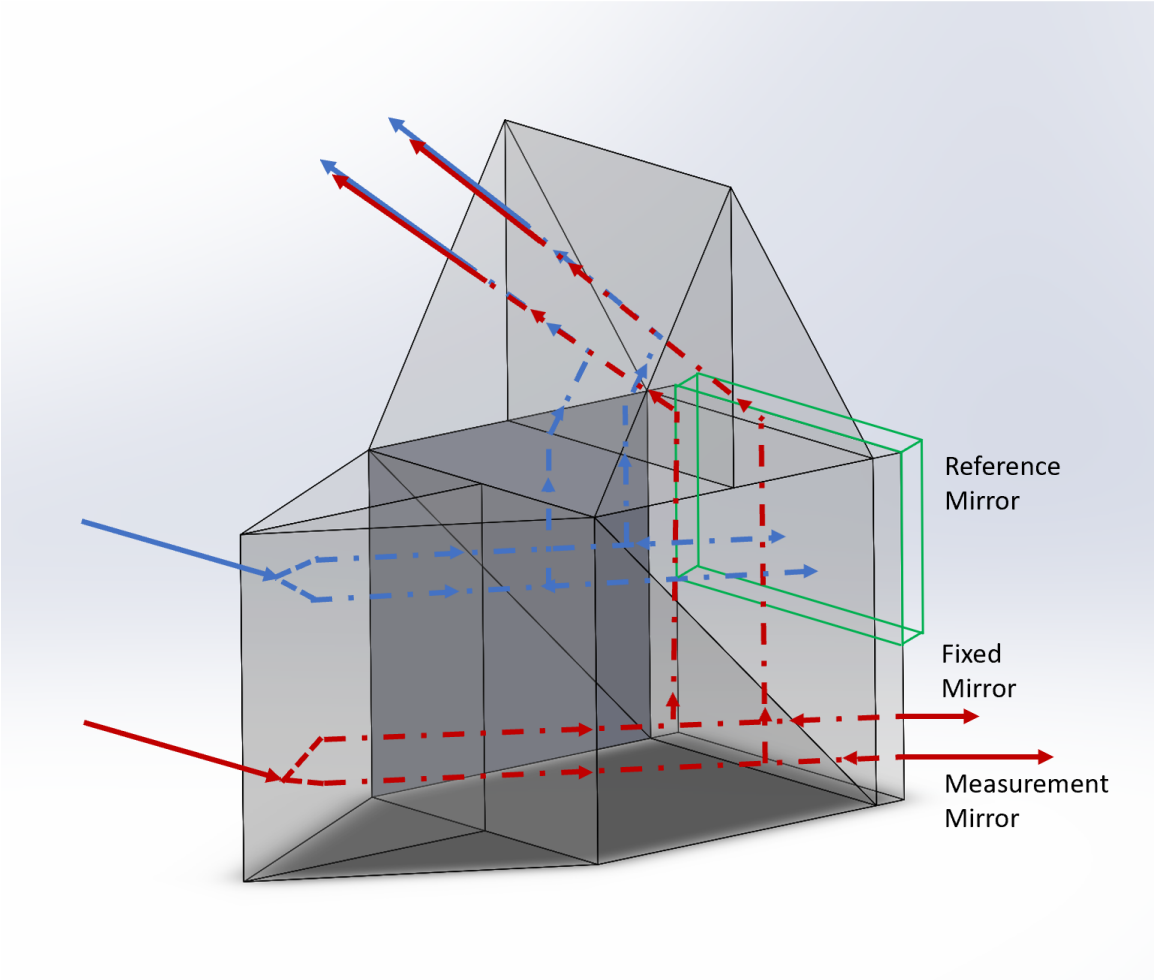

Figure 2.5: The optical path within the quasi-monolithic interferometer. The green cuboid represents where the reference mirror is attached to the interferometer unit. The output is read from the outputs from the top ETP.

The concept is similar to the one shown in Fig. 2.3. Details on the interferometer can be found in [2, 5].

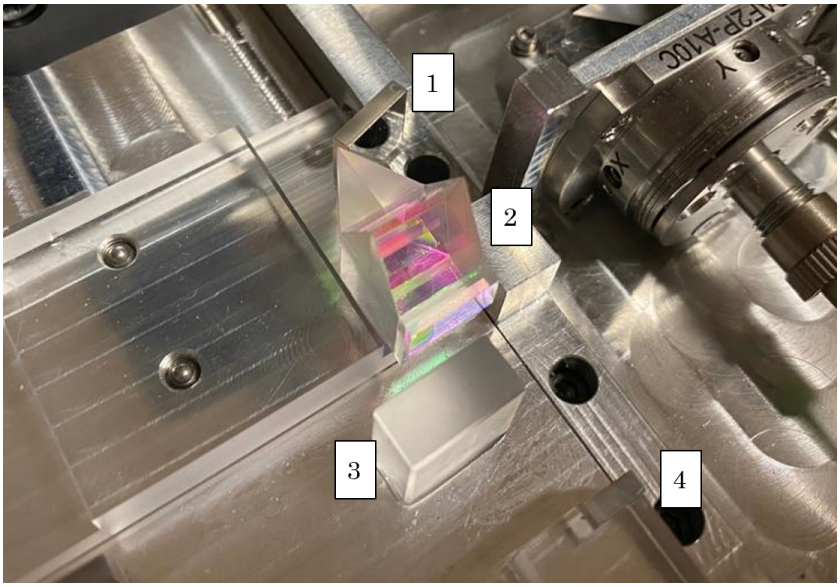

Figure 2.6:
Quasi-monolithic interferometer integrated with double resonator. This system is significantly more compact than the system for initial testing. 1 represents the angled mirror that guides beams into the quasi-monolithic unit, 2 is the interferometer unit itself, 3 is the reference mirror and 4 is the measurement mirror which is mounted to the 10 Hz test mass of the double resonator. This image is reprinted with permission from "Wide-band dual optomechanical resonators for inertial navigation" by Lee A. Capistran, Adam Hines, Jonathan Joseph Carter, Xiangyu Guo, Guillermo Valdes, Jose Sanjuan, Felipe Guzman Proceedings Volume 12447, Quantum Sensing, Imaging, and Precision Metrology; 1244718 (2023) SPIE Quantum West, 2023

The source for this interferometer is a 1550 nm laser and the frequencies driven through the AOMs for this interferometer are 39 and 40 MHz resulting in a heterodyne frequency of 1 MHz. This system is modeled after the compact heterodyne interferometer used for in air testing, but is compact and assembled as one single unit instead of multiple components used together. The attachments for the aluminum mount only accounted for the prism and collimators, so in order to lead beams into the interferometer an angled mirror had to be glued in place using UV glue along with the interferometer and reference mirror. These components can be seen in Fig. 2.6. In this case, the integrated quasi-monolithic system was used to take measurements of the 10 Hz test mass, and the fiber interferometer was integrated with the 50 Hz test mass.

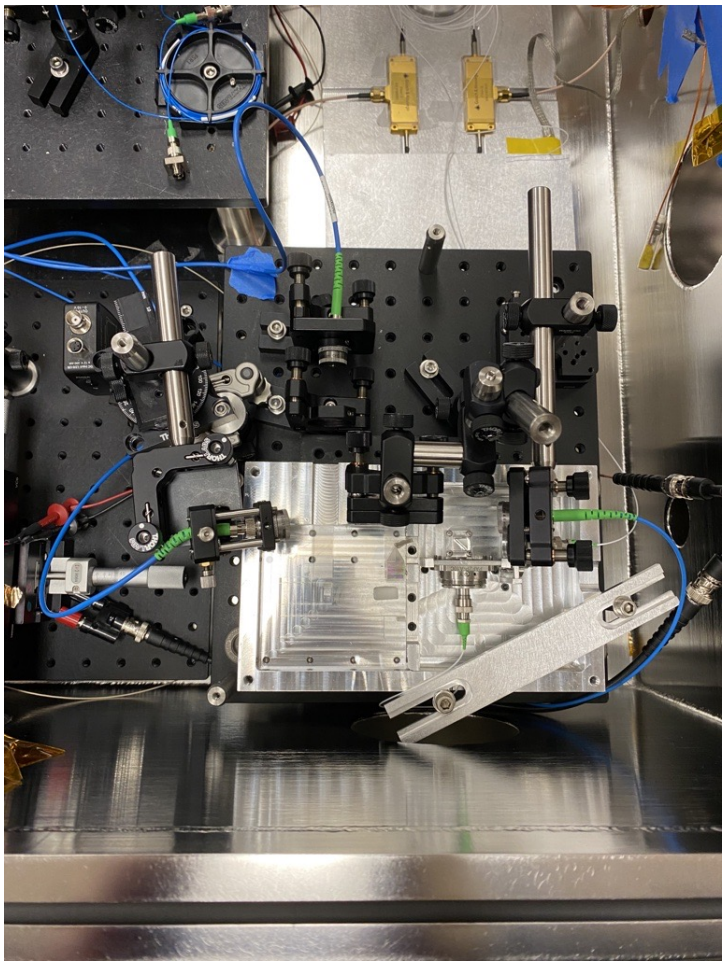

Figure 2.7: The resonator is resting in the aluminum mount along with the quasi-monolithic interferometer, the 90°prism. the two mounted collimators (which supply the beams to the 10 Hz resonator), the fiber interferometer is being provided to the 50 hz resonator. The other components on the bread board consists of collimators that where the output beams are being coupled to.

Finally, the signal we are interested in for all the interferometers is the difference in phase between the measurement interferometer and reference interferometer. This signal is generated when the resonator displaces. As it displaces back and forth it is changing the phase of the beam. This signal cancels out most of the common noise and should leave us with the motion of the test mass. The signal we are interested when taking measurements is delta phase: $\Delta\phi = \phi_m - \phi_r$. Where ϕ_m is the phase of the measurement arm and ϕ_r is the phase of the reference arm.

3. PRELIMINARY RESULTS*

[1] Quality factors of a system determine its ability to perform well. It defines the system's ratio of energy lost and energy stored. In other words, a high Q value means that the system loses energy at a slower rate, therefore resonating for a longer amount of time. A low Q would mean that the system resonates for a small amount of time not allowing for viable information to be taken. Two methods that can be used to obtain the Q of the system are ring down measurements and line-width measurements. The results presented are what was obtained from long term measurements of the test masses.

3.1 Results

Once the set up was in place, long term measurements of both test masses were taken simultaneously. This means measuring the displacement of the resonators over long periods of time with no intention of exciting the test mass. These measurements allowed to measure the line width, $\Delta\omega_0$, of the resonators and, consequently, their Q factor since:

$$Q = \frac{\omega_0}{\Delta\omega_0} \tag{3.1}$$

with $\omega_0 = 2\pi f_0$ the angular resonance frequency of the resonator. A transfer function can be defined as the relationship between an output and all the possible inputs of a system. In our case, relating acceleration and displacement measurements that are taken.The transfer function shown below can be applied to show the relationship between the displacement across all ωs and acceleration for those displacements.

$$\frac{x(\omega)}{a(\omega)} = \frac{-1}{\omega_0^2 - \omega^2 + i(\Gamma_v\omega + \omega_0^2\phi(\omega))} \tag{3.2}$$

[1]*Portions of this chapter are reprinted with permission from "Wide-band dual optomechanical resonators for inertial navigation" by Lee A. Capistran, Adam Hines, Jonathan Joseph Carter, Xiangyu Guo, Guillermo Valdes, Jose Sanjuan, Felipe Guzman Proceedings Volume 12447, Quantum Sensing, Imaging, and Precision Metrology; 1244718 (2023) SPIE Quantum West, 2023

The acceleration noise levels (in power spectral density, i.e., in units of $m^2\ s^{-2}$/Hz) are calculated as:

$$S_{a_{\mathrm{th}}}(\omega) = \frac{4k_{\mathrm{B}}T}{m\omega}(\Gamma_{\mathrm{v}}\omega + \omega_0^2\phi(\omega)) \tag{3.3}$$

where m represents the mass of the test mass, $\omega_0 = 2\pi f_0$ represents the resonators resonant frequency, Γ_{v} represents the velocity damping rate, k_{B} is the Boltzmann's constant, T is temperature in Kelvin, ω represents the angular frequency, and $\phi(\omega)$ is the mechanical losses experienced by the system including surface, bulk, thermal, elastic, and anchor losses.

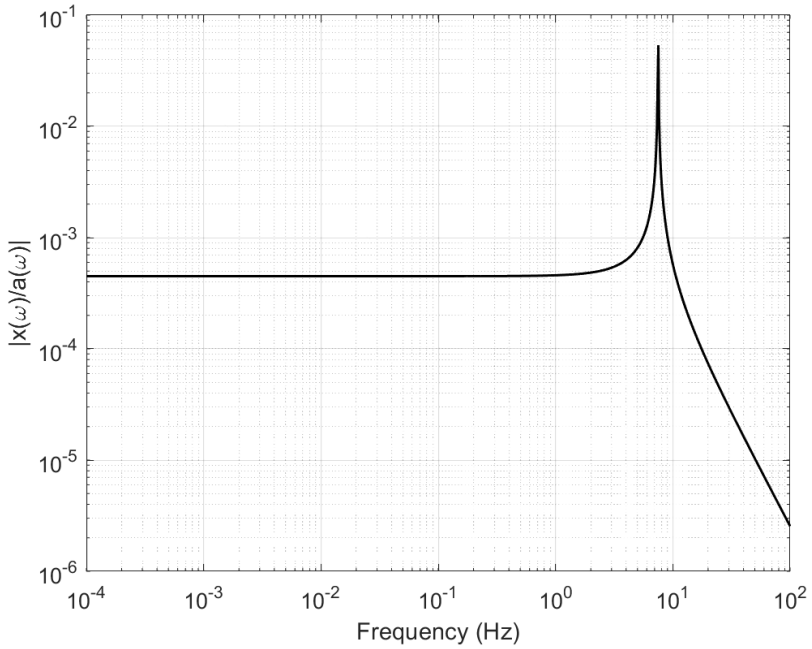

Figure 3.1: A visualization of the transfer function is presented using parameters f_0 = 7.5 Hz, ϕ = $1/Q$, $Q = 7.5$ x 10^5 and assuming Γ = 0 (or that system is in vacuum) will result in a plot such as this when plugging it into the transfer function and taking the absolute value.

3.1.1 Results in Air

Results in air for the both resonators were taken over a period of 8 hours, at a sampling rate of 122 Hz for the 10 Hz resonator and 488 Hz for the 50 Hz resonator at a bandwidth of 10 kHz

for both and are shown in Fig. 3.2 and Fig. 3.3. The resonance frequencies were close to the theoretical ones: 7.6 Hz and 48.7 Hz, respectively. The Q values were about 500 and 1500 for the low-frequency and high-frequency resonators, respectively. These values, although low, are expected due to the measurements being carried out in air, and thus dominated by Γ_{v}.

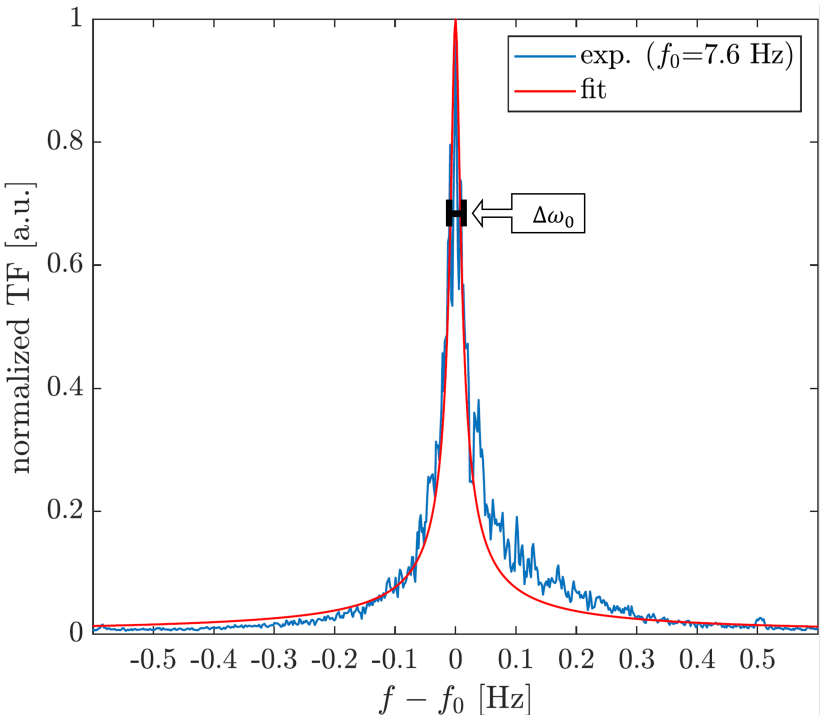

Figure 3.2: Plotting the normalized transfer function (TF) of the 10 Hz resonator response in vacuum gives us information about the true resonant frequency. While fitting a Lorentzian distribution allows us to find the FWHM or ω_0 divided by ω_0 – the ω that is 0.707 times max of the peak. This results in the Q of the 10 Hz resonator in air was 500 and the resonant frequency was found to be 7.6 Hz. This image is reprinted with permission from "Wide-band dual optomechanical resonators for inertial navigation" by Lee A. Capistran, Adam Hines, Jonathan Joseph Carter, Xiangyu Guo, Guillermo Valdes, Jose Sanjuan, Felipe Guzman Proceedings Volume 12447, Quantum Sensing, Imaging, and Precision Metrology; 1244718 (2023) SPIE Quantum West, 2023

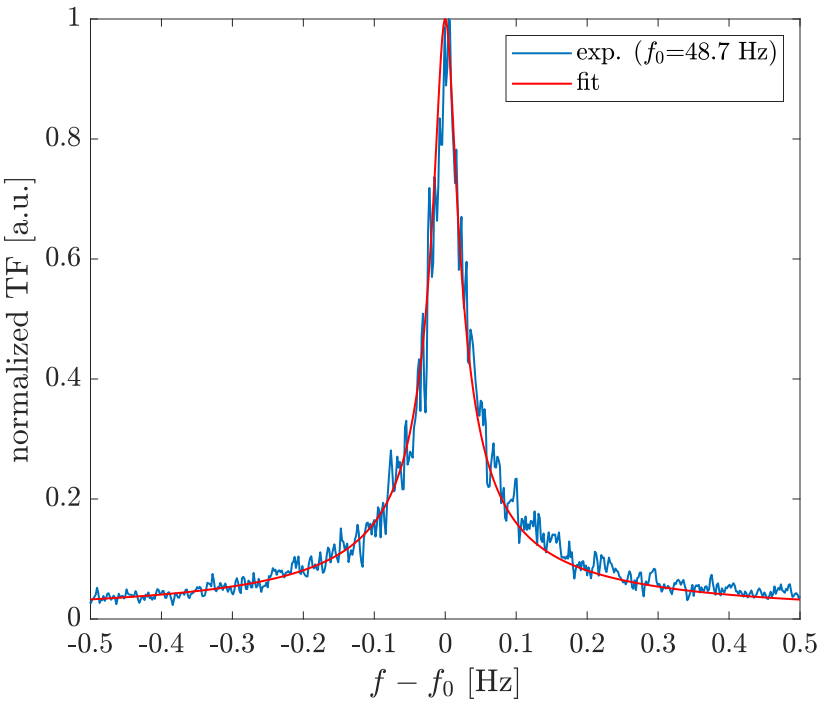

Figure 3.3: Using the methods stated before has resulted in the quality factor of the 50 Hz resonator was 1500 and the resonant frequency was found to be 48.7 Hz. This image is reprinted with permission from "Wide-band dual optomechanical resonators for inertial navigation" by Lee A. Capistran, Adam Hines, Jonathan Joseph Carter, Xiangyu Guo, Guillermo Valdes, Jose Sanjuan, Felipe Guzman Proceedings Volume 12447, Quantum Sensing, Imaging, and Precision Metrology; 1244718 (2023) SPIE Quantum West, 2023

Figure 3.4 shows the spectrum of the acceleration measured by both resonators simultaneously. Displacement from the interferometers is converted to acceleration using the resonators' transfer functions. The results between 5 and 15 Hz show large coherence, which indicates both accelerometers are measuring the same accelerations (i.e. vibrations from the laboratory). The panel in the bottom shows the coherence between the two traces in the top, which is almost perfect between 7 and 12 Hz. Identifying the coherence of the resonators' acceleration noise floors verifies the common surrounding vibrations in the lab. This benefits the system noise floor as both resonators received the same level of environmental noise and this can potentially be subtracted from our data post processing in order to characterize the inherent noise of the optomechanical resonators.

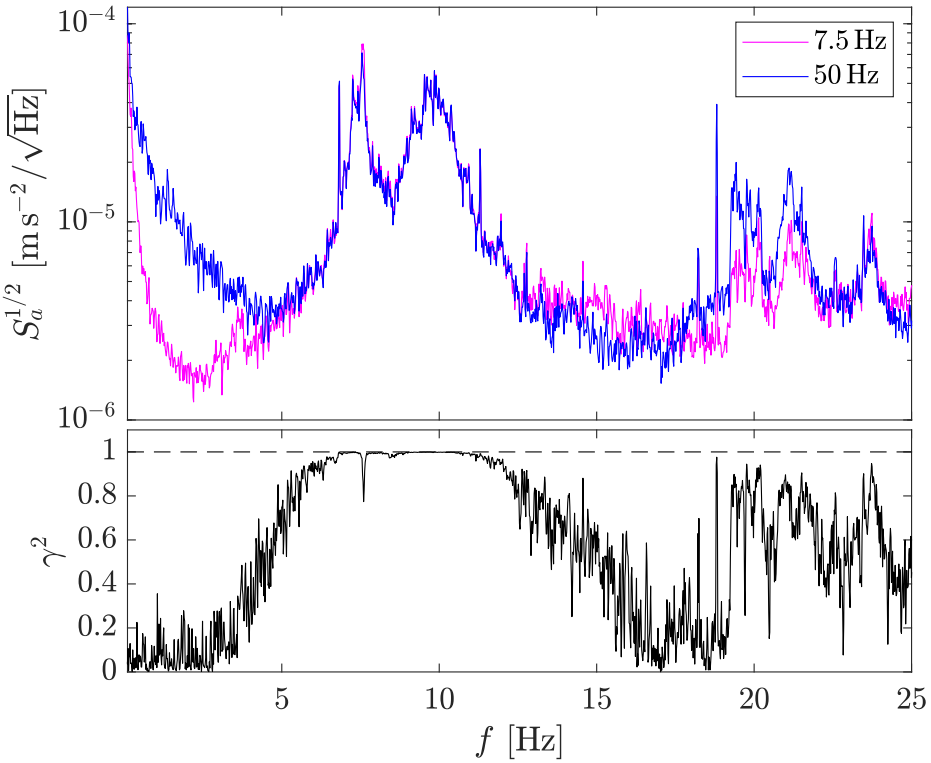

Figure 3.4: Top shows the acceleration spectral density (ASD) of laboratory vibrations measured with both resonators. Bottom shows coherence. This image is reprinted with permission from "Wide-band dual optomechanical resonators for inertial navigation" by Lee A. Capistran, Adam Hines, Jonathan Joseph Carter, Xiangyu Guo, Guillermo Valdes, Jose Sanjuan, Felipe Guzman Proceedings Volume 12447, Quantum Sensing, Imaging, and Precision Metrology; 1244718 (2023) SPIE Quantum West, 2023

3.1.2 Results in vacuum

A measurement in vacuum, at a pressure range of about 10^{-4} torr was carried out for 8 hours to measure the 10 Hz resonator's acceleration and 21 hours for the 50 Hz resonator. Preliminary measurements were performed using the same method of finding Q as in air. The same sampling rates and bandwidth were used for the in vacuum measurement. The Q values that resulted from these measurements are shown in Fig. 3.5 and Fig. 3.6. The resonance frequency changed slightly compared to the one in air (from 7.6 Hz to 7.74 Hz) and the qualify factor increased from 500 to about 800. The Q value in vacuum was expected to be significantly higher (in the $10^5 - 10^6$ range),

and efforts to understand this value are on-going.

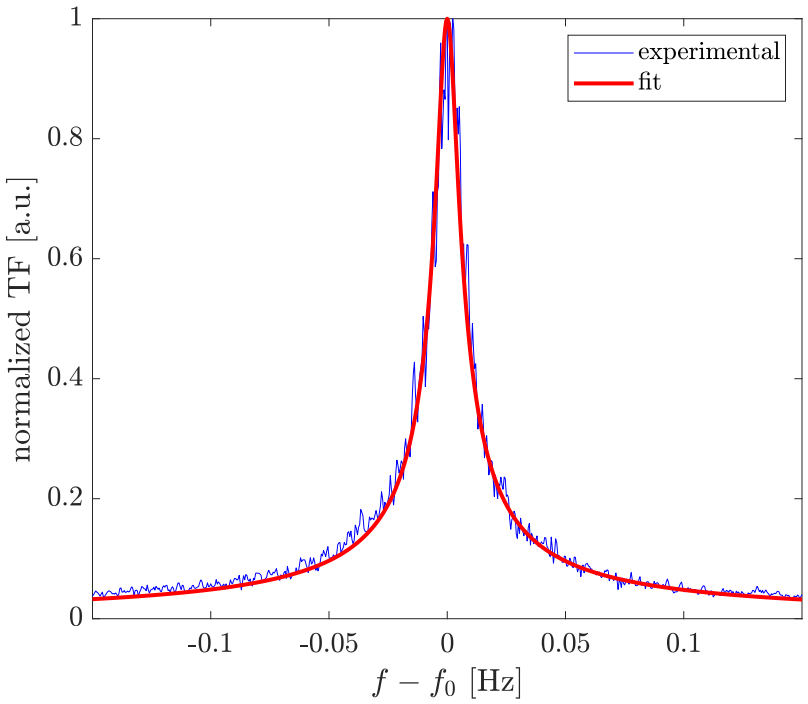

Figure 3.5: Using the methods stated before has resulted in the quality factor of the 10 Hz resonator to be 800 and the resonant frequency is 7.74 Hz. This image is reprinted with permission from "Wide-band dual optomechanical resonators for inertial navigation" by Lee A. Capistran, Adam Hines, Jonathan Joseph Carter, Xiangyu Guo, Guillermo Valdes, Jose Sanjuan, Felipe Guzman Proceedings Volume 12447, Quantum Sensing, Imaging, and Precision Metrology; 1244718 (2023) SPIE Quantum West, 2023

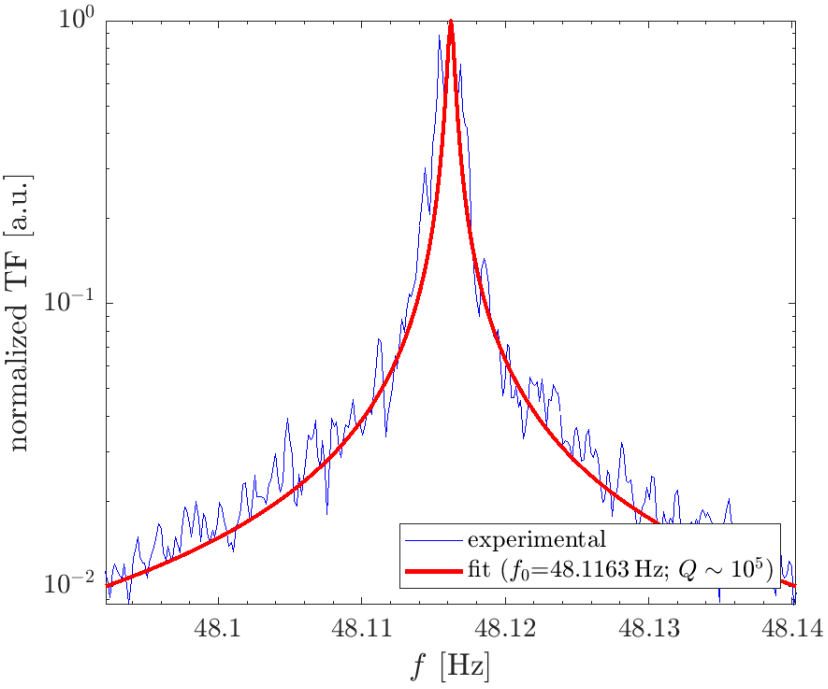

Figure 3.6: Using the methods stated before has resulted in the quality factor of the 50 Hz resonator to be about 100,000 and the resonant frequency is 48.1163 Hz.

The resonant frequency in vacuum was found to be 48.1163 Hz. The Q value in vacuum increased from 1500 to 100,000, which is expected due to the absence of Γ_v.

3.2 Noise projections

In this section we provide estimates of the noise limits of the dual resonator. The noise estimates are generated using theoretical Q values (in vacuum), and the Q values measured experimentally in air. It is expected for the noise floor in air to be less desirable, but in vacuum the noise floors are projected to improve. The theoretical Qs of both test masses are simulated based on noise models developed by the LIGO community [4, 6]. The theoretical values are 2.9×10^6 for the 10 Hz and 7.1×10^5 for the 50 Hz resonator.

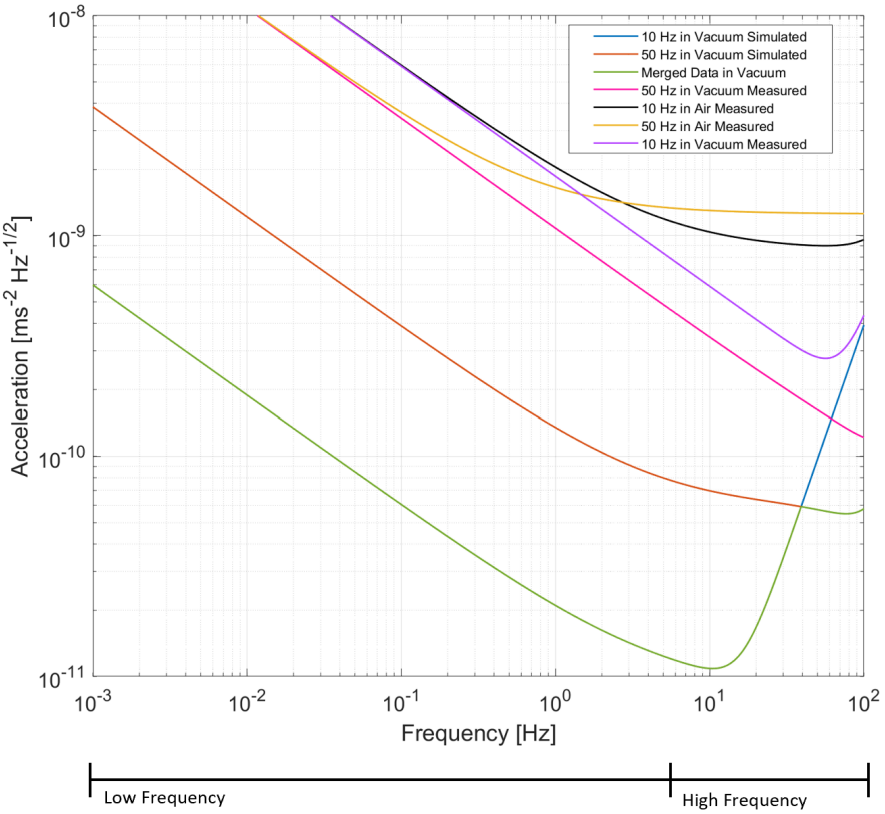

Figure 3.7: Projected noise floor measurements of both resonators when acceleration measurements are taken in air (with measured Qs) and in vacuum (with theoretical Qs). The merged data in air is not shown in this plot because it is dominated by the 10 Hz resonator in air. The noise floors that have been measured experimentally are also included with the Qs measured in vacuum. The label under the plot indicates the low and high frequency resonant range.

As expected, performance in air is worse than in vacuum conditions due to larger losses. From Fig. 3.7 one sees that the high-frequency resonator provides small advantages (or none for the in air condition). However, the results can be misleading since for frequencies near the resonance frequency and above one needs to know the transfer function of the resonator accurately in order to convert the displacement measurements into acceleration. That is at frequencies close to the resonant frequency, $(\omega_0 - \omega)$ approaches zero making the function dependent on Γ_v. Since $\Gamma_v = \omega_0 Q_{gas}$ having an accurate Q is essential in maintaining accuracy of the system's noise floor. For

this reason, even if the low-frequency resonator exhibits theoretical better performance in a wide frequency range, in practice, its use will be limited to $f < f_{0,\mathrm{low-freq}}$. The high-frequency resonator will be used in the frequency range from $f_{0,\mathrm{low-freq}}$ to $f_{0,\mathrm{high-freq}}$, i.e. from about 5 Hz to 45 Hz.

4. CONCLUSION

This chapter will cover the challenges that we have faced and the work that we plant to implement moving forward.

4.1 Challenges

The current challenges being faced are the mountings and optical equipment being used, which ultimately affect the amount of space it takes up. For example, we are currently using a combination of several kinematic mounts that allow for several degrees of freedom as our collimator mount at the quasi-monolithic output. This includes a rotational stage and linear track. This, however, has resulted in course alignment without fine tuning the position of the collimator meaning the position is not optimized. Using alternative mounting or optics could potentially improve results. Ideally, the quasi-monolithic interferometer would be used with the 50 Hz resonator because the 50 Hz resonator is less sensitive and requires an interferometer with higher sensitivity (such as the quasi-monolithic interferometer), but the double resonator has limited us to using the quasi-monolithic interferometer with the 10 Hz resonator instead. This being that the cutouts on the resonator plate would not allow for the bottom input beam to reach the quasi-monolithic interferometer when it is put in position to be used with the 50 Hz resonator. More importantly, the Q factor that we currently have for the 10 Hz resonator in vacuum is not what is expected according to the simulated Q values. Carrying out ring down measurements provides more accurate Q values for the system, however, excitation of the resonators has proven to be difficult when inside the chamber. In vacuum, we measured Q values on the order of 10^3, but we expected values in the range of 10^5 to 10^6. We know these numbers can be achieved as other researchers in our lab have measured Qs in the order of 10^5 before. [6]

4.2 Future Work

The immediate next steps include replacing optical mounting systems with more stable and precise mounting. This will allow for better positioning of the collimators used to couple the

output beams into our detectors. This new equipment will allow us to fine tune and optimize positioning and will consequently allow us to take simultaneous measurements of both resonators. Adding piezos to the system and driving it at appropriate voltages should excite the resonators and ring down measurements can then be taken. Measuring the decay of oscillations will then provide the Q of the system. When both resonators perform adequately alone, a measurement of both resonators will be taken simultaneously. This will allow us to measure the system's coherence in vacuum. In order to achieve levels of high sensitivity the system must have a low noise floor. Although estimates can be made, finding the source of noises or vibrations in the system could further reduce the noise floor. Having the sources of noise in our data means it can be subtracted post processing, closer revealing the true noise floor of the system itself. This can be seen in Ref. [7]. Finally, confirming the system's Q values, resonant frequencies, and noise floors are crucial to determining it's ability to perform as an inertial sensor for inertial navigation.

REFERENCES

[1] K.-N. Joo, E. Clark, Y. Zhang, J. D. Ellis, and F. Guzmán, "A compact high-precision periodic-error-free heterodyne interferometer," *J. Opt. Soc. Am. A*, vol. 37, pp. B11–B18, Sep 2020.

[2] Y. Zhang, "Optical readout systems for optomechanical inertial sensors," 2022.

[3] Y. Zhang and F. Guzman, "Fiber-based two-wavelength heterodyne laser interferometer," *Opt. Express*, vol. 30, pp. 37993–38008, Oct 2022.

[4] D. M. Macleod, S. Fairhurst, B. Hughey, A. P. Lundgren, L. Pekowsky, J. Rollins, and J. R. Smith, "Reducing the effect of seismic noise in ligo searches by targeted veto generation," *Classical and Quantum Gravity*, vol. 29, p. 055006, feb 2012.

[5] Y. Zhang and F. Guzman, "Quasi-monolithic heterodyne laser interferometer for inertial sensing," *Opt. Lett.*, vol. 47, pp. 5120–5123, Oct 2022.

[6] A. Hines, L. Richardson, H. Wisniewski, and F. Guzman, "Optomechanical inertial sensors," *Appl. Opt.*, vol. 59, pp. G167–G174, Aug 2020.

[7] A. Hines, *DEVELOPMENT OF AN OPTOMECHANICAL RESONATOR FOR LOW-FREQUENCY ACCELERATION SENSING*. PhD thesis, Texas A&M University, 2022.